ORIGINALARBEITEN/ORIGINALS

Reduction of wind turbine gearbox damage risk due to electrical faults via component design optimization

Julian Röder[1] · Georg Jacobs[1] · Dennis Bosse[1] · Fabian Herzog[1] · Aaron Zang[1]

Abstract

Over the lifetime of a wind turbine (WT) it is likely that several electrical faults occur. Electrical faults may induce significant electromagnetic generator torque excitations. The torque excitations are transferred to the gearbox components and lead to dynamic load changes as well as changes in the speed of rotation. Dynamic load changes in combination with changing rotational speeds might lead to gearbox component damage. Gearbox component damage is the main driver for WT downtime due to the high time to repair the fault. Especially the components of the high-speed stage (HSS) are prone to failure. This paper presents a method for introducing gearbox component design optimizations in order to reduce the damage risk during electrical faults. Via profile shift the HSS safety against scuffing cannot be further increased compared to the reference. The HSS safety against micropitting can be increased via profile shift by max. 41% and the safety against tooth flank fracture on the HSS by max. 3% compared to the reference. Via profile modification the HSS safety against scuffing can be increased by max. 14%, the HSS safety against micropitting by max. 8% and the safety against tooth flank fracture on the HSS by max. 8% compared to the reference. Via roller profile optimization the smearing risk on the HSS cylindrical roller bearing can be reduced by max. 3% compared to the reference. Thus, on the basis of two exemplarily analyzed electrical faults, this paper shows that gearbox component design optimizations can significantly reduce the gearbox damage risk during electrical faults.

✉ Julian Röder
   julian.roeder@cwd.rwth-aachen.de

[1] CWD, RWTH Aachen University,
   Campus-Boulevard 61, 52074 Aachen,
   Germany

Reduktion des Risiko für Getriebeschäden in Windenergieanlagen aufgrund von elektrischen Fehlern mittels Getriebedesignoptimierung

Zusammenfassung

Windenergieanlagen (WEA) unterliegen über ihre Lebensdauer statistisch mehreren elektrischen Fehler. Eletrische Fehler führen zu Stößen des elektromagnetischen Generatormoments. Die Generatormomentenstöße werden auf die Komponenten des Getriebes übertragen, weshalb es zu Last- und Drehzahlschwankungen kommt. Dynamische Lastschwankungen in Kombination mit schwankenden Drehzahlen können Schäden in den Getriebekomponenten hervorrufen. Schäden der WEA-Getriebekomponenten führen aufgrund der aufwändigen Reparaturmaßnahmen zu erheblichen Stillstandszeiten. Vorrangig von Schäden betroffen sind die Komponenten der schnelldrehenden Seite (HSS) des Getriebes. In diesem Artikel wird eine simulative Methode zur Untersuchung von Getriebedesignoptimierungen zur Reduktion des Risiko für Schäden während elektrischer Fehler vorgestellt. Mittels Profilverschiebung kann die Sicherheit gegen Fressen an der HSS im Vergleich zur Referenz nicht verbessert werden. Die Sicherheit gegen Mikropitting kann durch eine geeignete Profilverschiebung um max. 41 % im Vergleich zur Referenz gesteigert werden. Die Sicherheit gegen Flankenbruch kann mit Hilfe einer angepassten Profilverschiebung um max. 3 % verbessert werden. Mittels Zahnflankenkorrekturen kann die Sicherheit gegen Fressen um max. 14 %, die Sicherheit gegen Mikropitting um max. 8 % und die Sicherheit gegen Flankenbruch um max. 8 % im Vergleich zur Referenz erhöht werden. Eine Anpassung der Rollenprofilierung der HSS-Zylinderrollenlager führt zu einer Reduktion des Risiko für Anschmierungen von max. 3 % im Vergleich zur Referenz. Demnach zeigt dieser Artikel anhand zweier exemplarischer elektrischer Fehler für eine Forschungs-WEA, dass Designänderungen an den Getriebekomponenten zu einer signifikanten Reduktion des Schadensrisiko während elektrischer Fehler führen können.

1 Motivation

Wind energy is one pillar of the energy supply of the future. In order to encourage the installation of more WTs, costs need to continue to decline [1]. Apart from the initial investment (CAPEX) one major share for WT costs can be traced back to the gearbox reliability due to the high repair expenses. Hence, premature failures of gear wheels and bearings increase the levelized cost of energy (LCOE) [2]. The WT reliability can be improved if all loads during the lifetime are considered in the design process. Electrical faults can lead to dynamic generator torque excitations, which are not yet sufficiently considered in the current standards. The occurrence of grid faults is dependent on the nation's grid stability and its grid codes [3, 4]. For doubly fed induction generator (DFIG) WTs with partial scale power converter (PSC) grid faults are transmitted directly to the generator which results in torque excitations with amplitudes significantly higher than the rated torque (see Fig. 1a) [5]. Converter faults occur frequently compared to other WT faults [6] and lead to highly dynamic generator torque excitations (see Fig. 1b) [5, 7, 16]. For both load cases shown in Fig. 1 the faults as well as the occurring torque excitation and drivetrain kinematics are described in detail in previous publications [5, 9, 15].
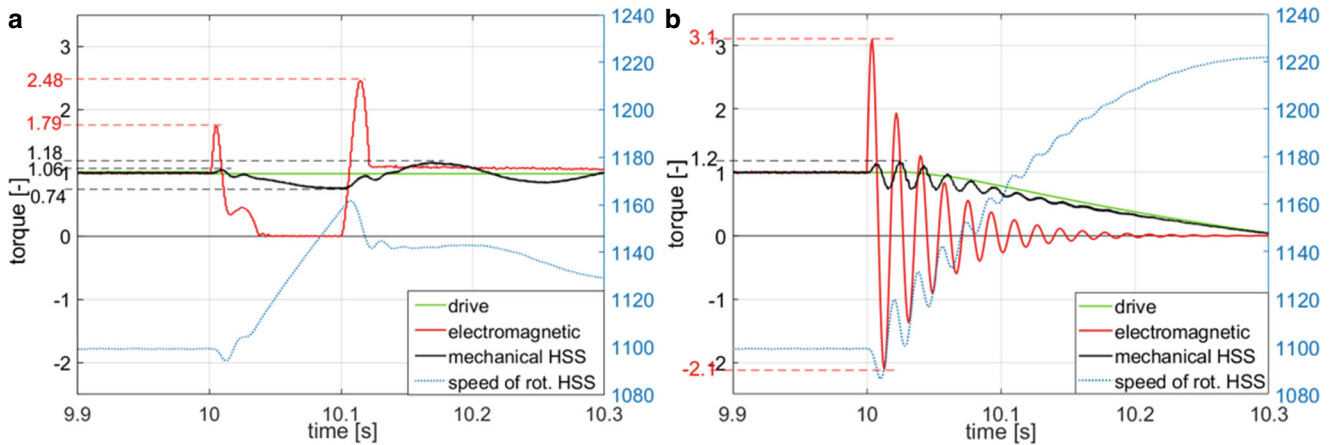
The torque excitations lead to a dynamic loading of the gearbox components which may result in an increase in the damage risk [5]. Gearbox damage occurs mainly on HSS bearings and gear wheels [8]. The generator torque excitations due to electrical faults have the highest influence on the HSS torque [9]. Research shows that the electrical faults increase the damage risk, e.g. for scuffing in the high-speed gear stage or for smearing in the HSS bearings [10]. Research also shows that the loading due to electrical faults and thus also the damage risk can be significantly reduced via electrical countermeasures [10, 11]. This paper evaluates gearbox component design changes for a damage risk reduction during electrical faults with regard to scuffing, micropitting and tooth flank fracture on the HSS gear wheel as well as smearing on a HSS cylindrical roller bearing via simulation.
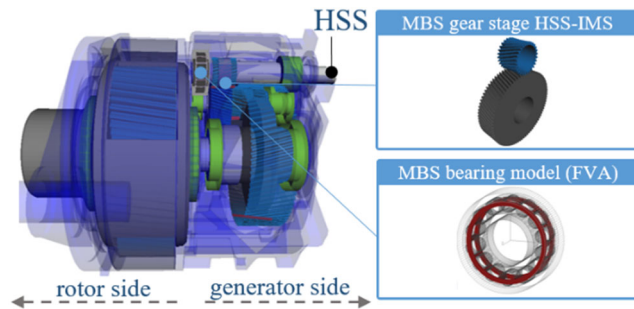
2 Approach

In this paper a simulative method for the effect evaluation of gearbox component design changes on the gearbox damage risks during electrical faults is shown. The effect of profile shift and tooth flank modification of the high-speed gear stage on scuffing, micropitting and tooth flank fracture as well as the impact of roller profile changes of a cylindrical roller bearing on the risk of smearing damage is investigated.

The torque excitations shown in Fig. 1 are generated via co-simulation of a DFIG WT with a grid fault and an FSC WT with a converter fault. These two electrical faults for both commonly used WT grid connection configurations are investigated in order to evaluate the effect of the gearbox component design changes holistically. A schematic overview and description of the co-simulation models including the faults can be found in previous publications [5,

Fig. 1 Torque excitation and HSS speed of rotation during: symmetrical grid fault with 5% remaining grid voltage and a duration of 100 ms for the reference DFIG WT (**a**) [5]; three-phase short circuit converter fault for the reference full size converter (FSC) WT (**b**) [5, 15] normalized by the torque during nominal operation and the gearbox ratio

Fig. 2 Gearbox model including the gear stage HSS-IMS and a detailed cylindrical roller bearing model

12, 13, 15]. The presented method can be applied to analyze any occurring electrical fault for WTs.

The central element of the co-simulation is a multi-body simulation (MBS) model of a research nacelle drivetrain [12, 13]. In order to gather the gearbox component loading a detailed MBS model of the gearbox is used (see Fig. 2). The gearbox model includes a detailed representation of the gear stages, including backlash and profile modification, as well as a detailed cylindrical roller bearing [14] at the HSS rotor side. With the help of this bearing model, forces and kinematics for each roller are calculated.

The MBS gearbox component load results are used as an input for damage criteria according to available standards and state-of-the-art publications. Doing so delivers safety values for scuffing, micropitting, tooth flank fracture and smearing. Via comparison of the safety values during the fault with and without the design change (reference) the effectiveness of each gearbox component design change is assessed.

3 Damage calculation methods

Using the MBS results it is possible to derive damage risk values for scuffing, micropitting and tooth flank fracture for the gear wheels and smearing for bearings. The damage calculation methods presented in this paper are based on currently available standards and state-of-the-art publications.

3.1 Scuffing

If thin elastohydrodynamic films occur in meshing gear teeth, asperity contact and subsequently scuffing might take place [16]. The safety against scuffing can be calculated via the flash temperature method according to ISO6336-20. The contact temperature Θ_B is defined as [16]:

$$\Theta_B = \Theta_M + \Theta_{fl} \tag{1}$$

Θ_M is the interfacial bulk temperature which can be approximated as the sum of the oil temperature Θ_{Oil}, the max. flash temperature $\Theta_{fl,max}$, the lubrication system factor X_S and the multiple mating pinion factor X_{mp}[16]:

$$\Theta_M = \Theta_{Oil} + 0.47 \cdot X_S \cdot X_{mp} \cdot \Theta_{fl,max} \tag{2}$$

Θ_{fl} is the flash temperature, which can be calculated via [16, 17]:

$$\Theta_{fl} = 2.52 \cdot \frac{\mu_m \cdot X_M \cdot X_J}{50} \cdot \sqrt[4]{(X_\Gamma \cdot w_{Bt})^3} \cdot \sqrt{\frac{n_1}{60}}$$
$$\cdot \frac{\text{abs}\left(\sqrt{\rho_{y1}} - \sqrt{\rho_{y2}/u}\right)}{\sqrt[4]{\rho_{rely}}} \tag{3}$$

where μ_m is the mean coefficient of friction, X_M is the thermo-elastic factor, X_J is the approach factor, X_Γ is the load sharing factor, w_{Bt} is the transverse unit load derived from the tangential force, n_1 is the speed of rotation of the pinion in rpm, ϱ_{y1} and ϱ_{y2} are the local radii of curvature of the pinion and gear wheel flank while ϱ_{rely} is the local relative radius of curvature.

The scuffing safety S_B can be calculated via the following formula using the experimentally determined scuffing temperature Θ_S [16]:

$$S_B = \frac{\Theta_S - \Theta_{\text{Oil}}}{\Theta_{B,\max} - \Theta_{\text{Oil}}} \tag{4}$$

3.2 Micropitting

Micropitting is influenced by the load, speed of rotation, temperature, specific lubricant film thickness as well as the lubricant itself and the surface topography [18]. Micropitting can be evaluated via ISO 6336-22. The calculation is based on the local specific lubricant film thickness $\lambda_{GF,Y}$ in the contact area and the permissible specific lubricant film thickness λ_{GFP}. Micropitting can occur, when the minimum specific lubricant film thickness $\lambda_{GF,min}$ is lower than λ_{GFP}. The local specific lubricant film thickness is the ratio of the local lubricant film thickness h_Y, and the effective arithmetic mean roughness value Ra [18]:

$$\lambda_{GF,Y} = \frac{h_Y}{Ra} \tag{5}$$

The local lubricant film thickness h_Y is defined as the product of normal radius of relative curvature at point Y on the path of contact $\varrho_{n,Y}$, material parameter G_M, local velocity parameter U_Y, local load parameter W_Y and local sliding parameter $S_{GF,Y}$ [18]:

$$h_Y = 1600 \cdot \rho_{n,Y} \cdot G_M^{0,6} \cdot U_Y^{0,7} \cdot W_Y^{-0,13} \cdot S_{GF,Y}^{0,22} \tag{6}$$

Table 1 Investigated profile shift coefficients for the HSS and IMS

Profile shift coefficient:	HSS	IMS
Reference	+0.110	+0.209
$x_{HSS,dec2}$	–0.637	+0.956
$x_{HSS,dec1}$	–0.263	+0.583
$x_{HSS,inc1}$	+0.544	–0.224
$x_{HSS,inc2}$	+0.977	–0.658

The safety against micropitting can be formulated as follows [18]:

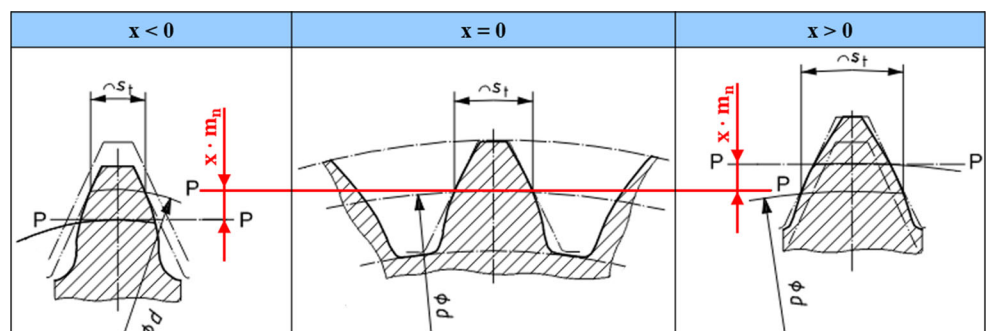$$S_\lambda = \frac{\lambda_{GF,\min}}{\lambda_{GFP}} \tag{7}$$

3.3 Tooth flank fracture

Tooth flank fracture is a complex interaction of stress fluctuations and material inhomogeneities. It is characterized by a primary fatigue crack in the region of the active contact area typically at a considerable depth below the surface. The primary crack propagates towards the surface of the loaded flank and towards the opposite tooth root section. The final breakage of the tooth is due to forced rupture [19]. The tooth flank fracture load capacity calculation according to ISO6336-4 allows a calculation of the local material exposure with a small set of parameters [19]. The local material exposure $A_{FF,CP}$ in the material depth perpendicular to the tangential contact y for every point on the path of contact can be calculated via [19]:
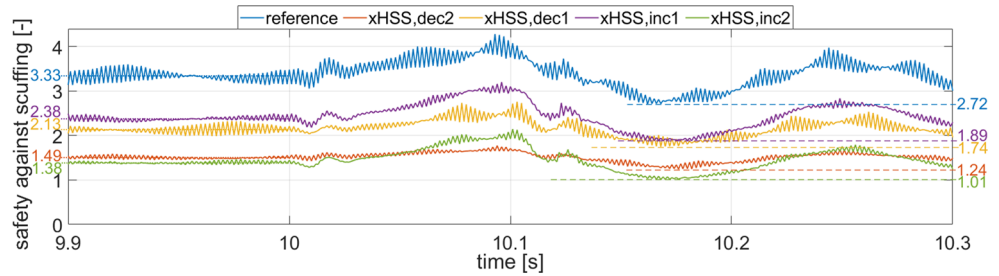
$$A_{FF,CP}(y) = \frac{\tau_{\text{eff},CP}(y)}{\tau_{\text{per},CP}(y)} + c_1 \tag{8}$$

$\tau_{eff,CP}$ represents the local equivalent stress and $\tau_{per,CP}$ stands for the local material shear strength for the contact point. The constant c_1 is defined as the material exposure calibration factor, which is 0.04 for case carburized steels. The local equivalent stress is calculated based on the local occurring equivalent stress $\tau_{\text{eff},L,CP}$, the influence of the residual
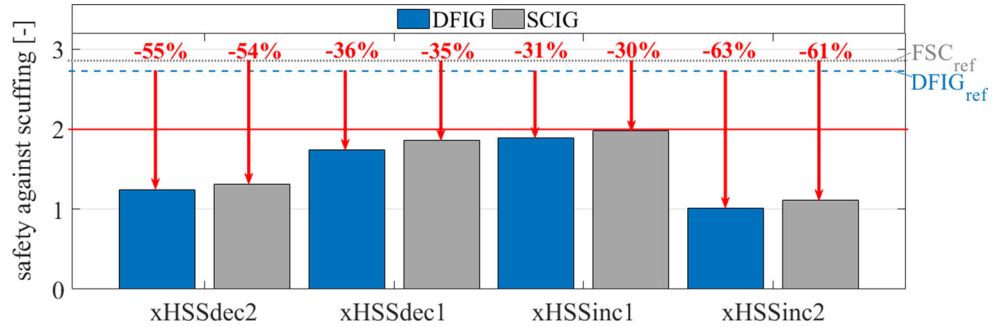
Fig. 3 Schematic overview of a gear tooth with different profile shift coefficients according to DIN ISO 21771 [22]

Fig. 4 Safety against scuffing on the HSS gear wheel for different profile shifts for the DFIG WT

Fig. 5 Min. scuffing safety on the HSS gear wheel for the profile shifts compared to the reference during the fault for both load cases (see Fig. 1)

stresses on the local equivalent stress $\Delta\tau_{\text{eff},L,RS,CP}$ and the quasi-stationary residual stress $\tau_{eff,RS}$ [19]:

$$\tau_{\text{eff},CP}(y) = \tau_{\text{eff},L,CP}(y) - \Delta\tau_{\text{eff},L,RS,CP}(y) \\ - \tau_{\text{eff},RS}(y) \tag{9}$$

The local material shear strength $\tau_{per,CP}$ for every contact point consists of the hardness conversion factor $K_{\tau,per}$, the material factor $K_{material}$ and the hardness HV [20]:

$$\tau_{\text{per},CP}(y) = K_{\tau,\text{per}} \cdot K_{\text{material}} \cdot HV(y) \tag{10}$$

$A_{FF,max}$ is defined as the maximum calculated local material exposure, where y is equal to or greater than half of the Hertzian contact width [19]:

$$A_{FF,\max} = \max\left[A_{FF,CP}(y)\right] \tag{11}$$

Experimental investigations on case carburized gears have shown, that a maximum material exposure $A_{FF,\max} \geq 0{,}8$ may cause tooth flank fracture under constant input torque [19]. Thus, the safety against tooth flank fracture can be defined as follows:

$$S_A = \frac{0.8}{\max\left[A_{FF,CP}(y)\right]} \tag{12}$$

3.4 Smearing

Smearing damage is based on adhesive wear [20]. Smearing damage is triggered by a combination of high loading and changing rotation speeds due to an increase in the in-

troduced power P per loaded area A. The smearing criterion used in this paper is shown in the following equation [21]:

$$\left(\frac{P}{A}\right)_{\max} = \\ \max\left\{0.5 \cdot \mu(t) \cdot p_{\max}(t) \cdot [u_1(t) - u_2(t)]\right\} \tag{13}$$

μ is the friction coefficient, p_{max} is the max. Hertzian contact pressure and u_1–u_2 is the circumferential contact velocity difference between roller and raceway.
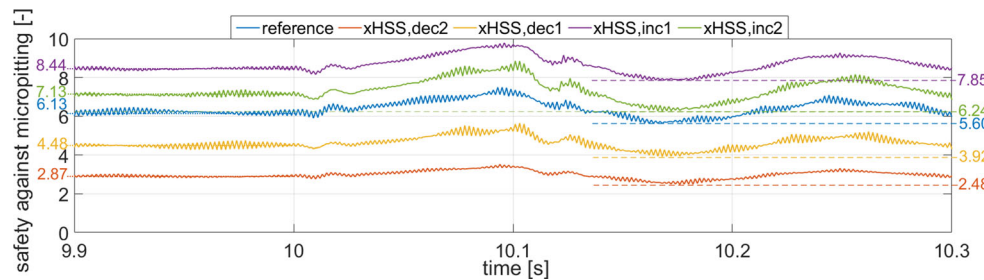
4 Results

Due to the vast number of gearbox component design parameters this paper only shows a selection. Profile shift and tooth flank modification are evaluated for the high-speed gear stage. For the rotor side HSS cylindrical roller bearing different roller profiles are investigated.
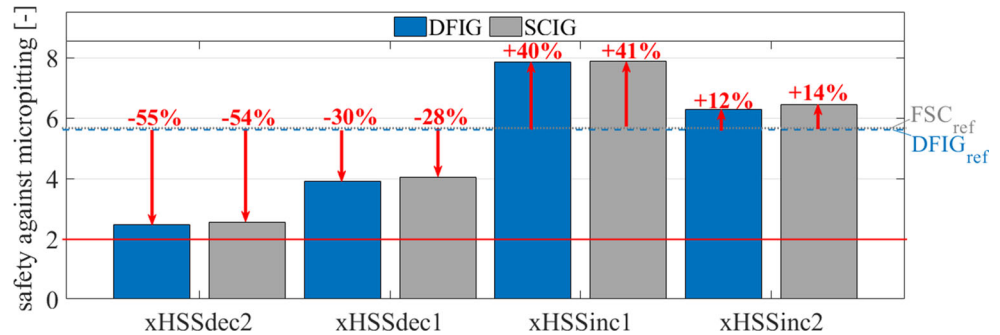
4.1 Profile shift

The displacement of the basic rack datum line from the reference cylinder of an involute gear is defined as profile shift $x \cdot m_n$ (see Fig. 3), with the profile shift coefficient x and the normal module m_n [22]. Profile shift influences the loading and the relative contact velocity of each gear wheel. The transverse tooth thickness on the reference circle s_t of the shifted tooth decreases for $x < 0$ and increases for $x > 0$ [22]. Since the involute geometry of the gear tooth is solely dependent on d and d is independent of x, the shape
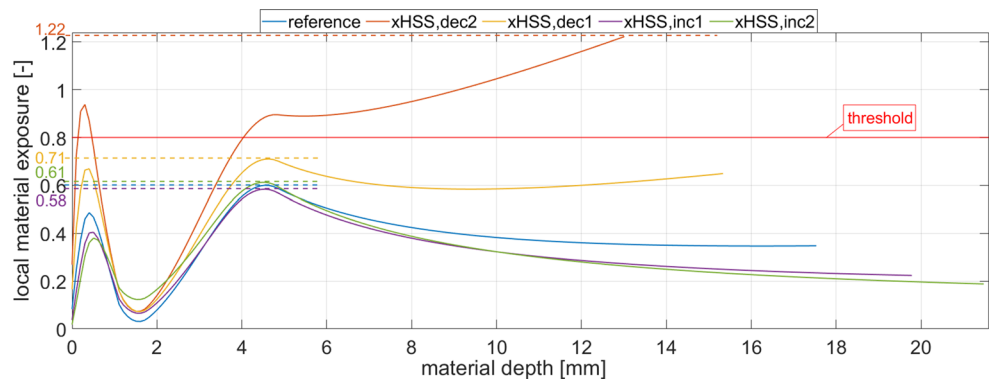
Fig. 6 Safety against micropitting on the HSS gear wheel for different profile shifts for the DFIG WT
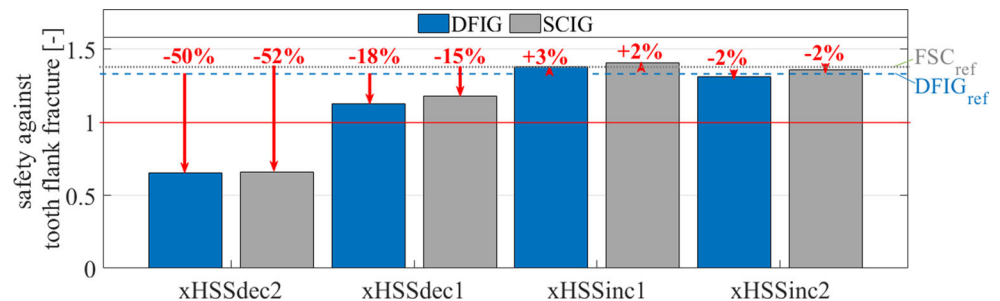

Fig. 7 Min. safety against micropitting on the HSS gear wheel for different profile shifts compared to the reference during the fault for both load cases (see Fig. 1)

Fig. 8 HSS gear wheel material exposure for different profile shifts at the critical point in time for the DFIG WT

Fig. 9 Min. safety against tooth flank fracture of the HSS gear wheel for different profile shifts compared to the reference during the fault for both load cases (see Fig. 1)
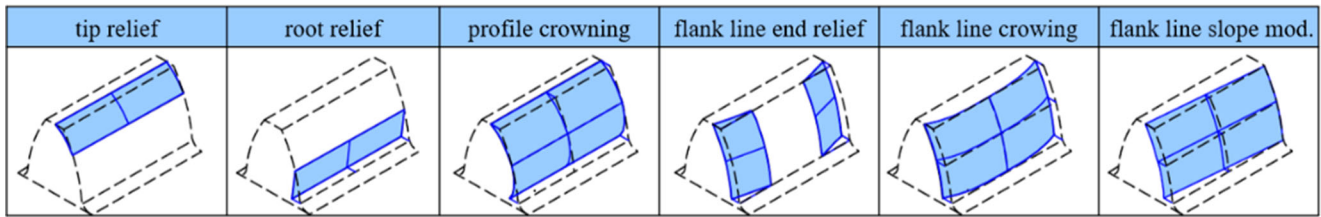

of the tooth flank does not change but a different section of the involute is used for different profile shifts [22].

One reason for the use of profile shift is the ability to distribute the loading optimally to pinion and gear wheel [22]. The investigated profile shift coefficients are given in Table 1.

In Fig. 4 the safety against scuffing on the HSS gear wheel for the given profile shifts is shown exemplarily for the DFIG WT load case presented in Fig. 1. $x_{HSS,inc2}$ and $x_{HSS,dec2}$ have the lowest safety against scuffing during the fault (1.01 and 1.24). Since the standard advices to have safety values of at least 2 [16], these designs are not sufficient with regard to scuffing damage. Also $x_{HSS,inc1}$ and $x_{HSS,dec1}$ are slightly below the advised safety threshold (1.89 and 1.74). Thus, both an increase and a decrease in HSS profile shift coefficient leads to a significant increase in the scuffing risk. Subsequently, the reference profile shift is already the optimum (2.72), if profile shift is regarded

Fig. 10 Schematic overview of the investigated tooth flank modifications [22]

individually. The contact temperature is based on the flash temperature and the interfacial bulk temperature (see Eq. 1). Both are influenced by the Hertzian contact pressure and the relative contact velocity. The relative contact velocity steadily increases for increasing HSS profile shift coefficients compared to the reference while the Hertzian contact pressure decreases for increasing HSS profile shift coefficients (see Fig. 3). Thus, there is an opposing effect of contact velocity and Hertzian contact pressure with an optimum at a certain profile shift. The results regarding the minimum safety values for all profile shifts are summarized in Fig. 5.

In conclusion, it was shown that via solely changing the profile shift the HSS scuffing risk during electrical faults cannot be decreased since all safety values are reduced compared to the reference.

The standard advices to also change the tooth flank modification as soon as the profile shift coefficients reach a certain threshold in order to cope with, e.g. problems at the tooth tip via introducing tip relief. Adding sufficient tooth flank modification leads to improved load sharing factors

X_Γ (see Eq. 3) and as a result, to larger safety values [16]. Note that the standard does not differentiate continuously with regard to X_Γ, but rather introduces a distinction of cases, where at a certain point of profile shift the default X_Γ is replaced with an ideal one, which significantly improves the safety via reduction of edge loading [16]. Tooth flank modification is described in Sect. 4.2. A detailed analysis of combined changes of profile shift and profile modification, their interdependencies and their influence on all damage criteria via a multi factorial sensitivity analysis will be part of future works.

Similar analysis as for scuffing can be done for the safety against micropitting (see Fig. 6, exemplarily analyzed for the DFIG WT load case shown in Fig. 1).

As can be seen, the safety values are all above 2. Therefore, all designs are sufficient with regard to micropitting damage. An increasing HSS profile shift coefficient leads to an increase in HSS safety against micropitting (6.24 and 7.85), while a decrease reduces the safety (3.92 and 2.48) compared to the reference (5.60). With increasing HSS profile shift coefficient also $\varrho_{n,Y}$ increases, which influences h_Y
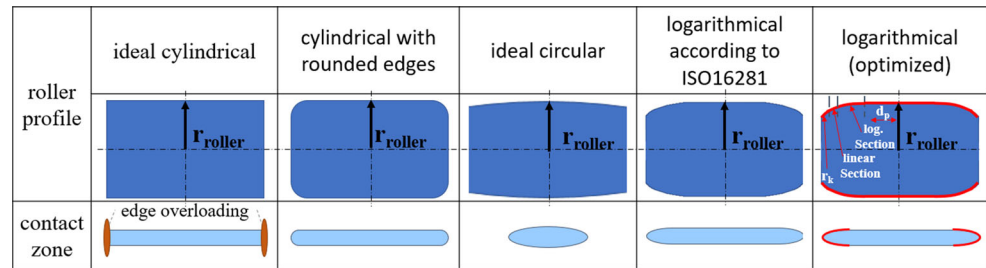
Table 2 Definition of the investigated HSS-IMS gear pairs tooth flank modification ranges

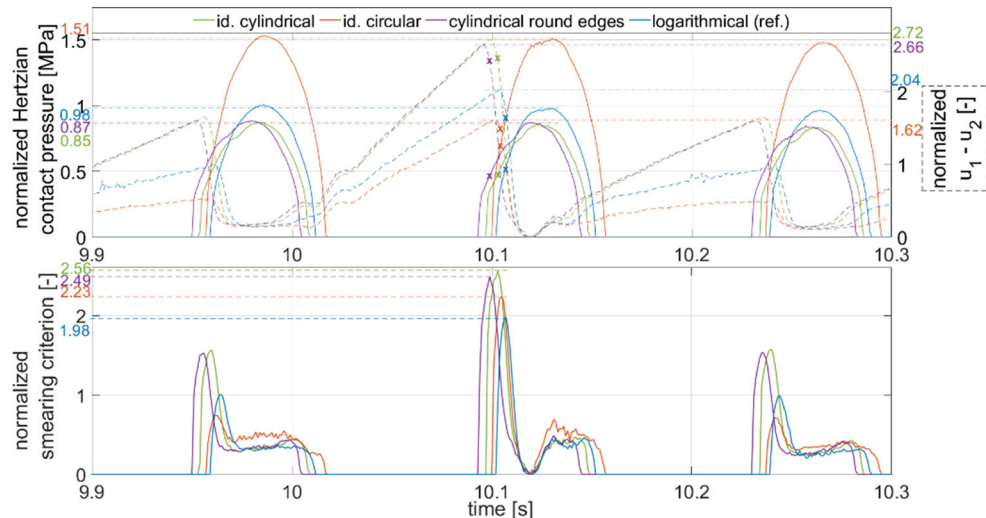| Modification type	Parameter	Reference values, HSS | IMS	Modification range, HSS | IMS
Tip relief	$C_{\alpha a}$— tip relief amount	(40 | 30) µm	(40 to 200 | 30 to 150) µm
Root relief	$C_{\alpha f}$— root relief amount	(0 | 0) µm	(0 to 40 | 0 to 40) µm
Profile crowning	C_α— profile crowning amount	(20 | 0) µm	(20 to 100 | 0) µm
Flank line end relief	$C_{\beta I;II}$— end relief amount (datum; non-datum face)	(0.0 | 25;35) µm	(0.0 | 25 to 125;35 to 70) µm
Flank line crowning	C_β— flank line crowing amount	(50 | 0) µm	(50 to 250 | 0) µm
Flank line slope modification	$C_{H\beta}$— flank line slope amount	(0.111 | 0.111) mrad	(–0.332 to 0.553 | –0.332 to 0.553) mrad

Table 3 Summary of the results regarding tooth flank modification; values are given for the most critical point during the fault for both load cases (see Fig. 1) as percentage change compared to the reference

Modification type	DFIG: scuffing | micropitting | tooth flank fracture	SCIG: scuffing | micropitting | tooth flank fracture
Reference safety values	2.72 | 5.60 | 1.33	2.89 | 5.82 | 1.39
Tip relief	+14 | +8 | +8	+13 | +7 | +8
Root relief	0 | 0 | 0	0 | 0 | 0
Profile crowning	+9 | +5 | +8	+7 | +4 | +6
Flank line end relief	0 | 0 | 0	0 | 0 | 0
Flank line crowning	0 | 0 | 0	0 | 0 | 0
Flank line slope mod	+7 | +4 | +6	+8 | +3 | +5

Fig. 11 Schematic overview of the investigated roller profiles and corresponding contact zone

Fig. 12 Max. Hertzian contact pressure, difference of circumferential velocity and smearing criterion normalized by the value of the reference profile during normal operation

linearly (see Eq. 6). Subsequently, the safety against micropitting is increased. At a certain point an increase in HSS profile shift coefficient does not increase the safety anymore (compare $x_{HSS,inc1}$ and $x_{HSS,inc2}$ in Fig. 7). For increasing HSS profile shift coefficients the transverse contact ratio decreases. Subsequently, also h_Y decreases. Thus, there is an opposing effect of $\varrho_{n,Y}$ and the transverse contact ratio for increasing HSS profile shift coefficients, which leads to the better safety for $x_{HSS,inc1}$ compared to $x_{HSS,inc2}$.

In conclusion, it was shown that via changing the profile shift it is possible to decrease the HSS micropitting risk during electrical faults. The proposed design choice regarding HSS micropitting safety should be in the direction of $x_{HSS,inc1}$.

In order to evaluate tooth flank fracture risk, the material exposure needs to be investigated (see Fig. 8, exemplarily shown for the DFIG WT load case presented in Fig. 1). $x_{HSS,dec2}$ leads to an overshoot of the threshold of 0.8 and therefore the design is not sufficient. Tooth flank fracture is a complex interaction of stress fluctuations and material inhomogeneities. Since a decreased HSS profile shift coefficient leads to a shift of the loaded tooth area to a small area at the tooth tip (see Fig. 3) the Hertzian contact pressure increases, which leads to the large increase in material exposure. The increased profile shift coefficients do not change the material exposure significantly (0.58 and 0.61) compared to the reference (0.60).

In Fig. 9 the results regarding safety against tooth flank fracture are summarized for both above-mentioned load cases. As can be seen, only $x_{HSS,dec2}$ is not sufficiently designed against tooth flank fracture.

In conclusion, it was shown that via changing the profile shift it is possible to mitigate the HSS tooth flank fracture risk during electrical faults. The HSS profile shift coefficient should not be decreased more than $x_{HSS,dec1}$.
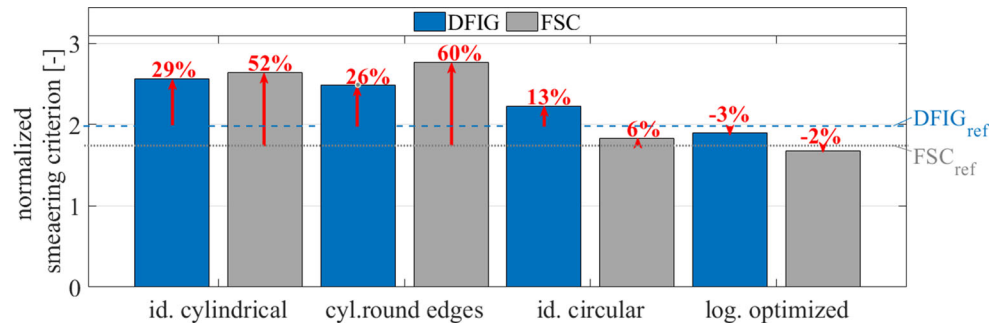
4.2 Tooth flank modification

Tooth flank modifications alter the tooth flank compared to the reference involute geometry [22]. Figure 10 shows the tooth flank modifications investigated in this paper.

In Table 2 the investigated parameter ranges are shown. Note that the profile modifications are applied symmetrically, i.e. similar for left and right tooth flank.

The results regarding tooth flank modification are summarized in Table 3 for scuffing, micropitting and tooth flank fracture. Note that only percentage change values are given, for which the modification leads to an increase in safety. Otherwise, the value is 0. As can be seen, only tip relief, profile crowning and flank line slope modification lead to an improvement compared to the reference. Thus, the reference modification is already suited well to cope with the normal operating conditions as well as the electrical faults. In order to set the reference into perspective, note that the

Fig. 13 Max. smearing criterion for the different roller profiles compared to the reference during the fault

safety values for scuffing, micropitting and tooth flank fracture are reduced by 31, 19 and 29% if no modification is applied.

In conclusion, it was shown that via tooth flank modification the HSS gear wheel damage safety during electrical faults can be improved. The proposed design choice is the reference modification with a slight tip relief increase (120 µm HSS, 90 µm IMS), larger profile crowning (100 µm HSS, 0 µm IMS) and larger flank line slope modification (0.33165 mrad HSS, 0.33165 mrad IMS).

4.3 Roller profile

The roller profile of a cylindrical roller bearing has a significant influence on the load distribution over the roller length (see Fig. 11) and the slip behavior.

The ideal cylindrical profile has an overloading at the edges of the roller which can significantly reduce the lifetime of the bearing [23, 24]. To mitigate the effect of edge overloading edge radii can be introduced [23, 24]. The ideal circular profile has the smallest contact zone due to the point contact [23]. A widely used profile type is the logarithmical profile according to ISO 16281 [24]. Also, the reference has a logarithmical profile. In order to optimize this profile, the parameters of the logarithmical function, e.g. the constant multiplication factor a_p, the length of the linear section d_p and the edge radius r_k, can be varied.

In Fig. 12 p_{max}, u_1–u_2 and the smearing criterion are shown for the different roller profiles exemplarily for the DFIG WT with the grid fault (Fig. 1a).

The critical point for smearing is a point of large p_{max} while u_1–u_2 is still elevated. This point occurs especially in the acceleration phase of the roller. The values of p_{max} and u_1–u_2 which correspond to the peak values of the smearing criterion are marked via crosses in Fig. 12. It can be seen that the logarithmical reference profile has the smallest smearing criterion increase during the fault to around 1.98 times the value during normal operation. The criterion for the ideal circular profile increases to around 2.23 times the value of the reference profile during normal operation. This is due to the large increase in p_{max} while u_1–u_2 is only slightly decreased compared to the reference. The smear-

ing criterion for the ideal cylindrical profile increases during the fault to around 2.56 times and for the cylindrical profile with rounded edges to around 2.49 times the value of the reference during normal operation due to the larger contact zone and the resulting increased u_1–u_2.

In order to improve the reference, an optimization of the logarithmic profile (see Fig. 11) is evaluated. An increase in the constant multiplication factor a_p leads to a steeper logarithmical section. Thus, the contact zone is slightly smaller, u_1–u_2 is decreased and consequently the smearing criterion decreases by max. 3%. Since d_p is already at zero for the reference, it can only be increased. An increase leads to a larger contact zone and larger u_1–u_2. Thus, an increase of d_p leads to an increased smearing criterion. r_k is 2.3 mm for the reference. Since the radius does not affect the loading and u_1–u_2 significantly as long as the logarithmic section is sufficient, r_k does not significantly influence the smearing risk.

In Fig. 13 the results for both above-mentioned load cases and all profiles including the best optimized logarithmical profile are summarized.

In conclusion the best profile regarding smearing is a logarithmic profile. Via parameter changes of the logarithmic profile it is possible to further reduce the smearing risk by max. 3% during the electrical faults.

5 Conclusion

Electrical faults can increase the damage risks of gearbox components and therefore reduce the LCOE. Countermeasures can be applied in order to reduce the loading due to the faults and thereby also reduce the damage risk. In this paper a simulative method for introducing gearbox component design optimizations in order to reduce the damage risk during electrical faults is evaluated on the basis of two exemplary load cases. Via profile shift the HSS gear wheel safety against scuffing cannot be further increased compared to the reference. The HSS safety against micropitting can be increased via profile shift by max. 41% and the safety against tooth flank fracture on the HSS gear wheel by max. 3% compared to the reference. Via profile modification the

HSS gear wheel safety against scuffing can be increased by 14%, the HSS safety against micropitting can be increased by max. 8% and the safety against tooth flank fracture on the HSS gear wheel by max. 8% compared to the reference. The lowest risk of smearing on the HSS cylindrical roller bearing occurs for the reference logarithmic profile. It can be further reduced via optimizing the logarithmical profile by max. 3%.

Thus, this paper shows the possibility to significantly reduce the gearbox component damage risks during electrical faults via improving the component parameters.

6 Outlook

In this paper, two electrical faults were analyzed in order to show the applicability of the presented method exemplarily. In future works all possibly occurring electrical faults need to be analyzed combined in order to find the final design.

Furthermore, in order to evaluate the overall effectiveness of a design change, i.e. considering all damage criteria combined and also the interdependencies between e.g. profile shift and tooth flank modification, while simultaneously achieving the best dynamic behavior during normal operation, a multifactorial sensitivity analysis needs to be done in future works.

Knowing the effectiveness of each countermeasure an informed decision about the financial feasibility can be made. A detailed cost analysis will be part of future works.

Besides gearbox component design changes also the structural elements of the gearbox have an influence on the damage risks during electrical faults due to e.g. larger induced misalignment. Thus, it is necessary to investigate the stiffness of the gearbox shafts, the bearings and the housing. Furthermore, the coupling between the gearbox and the generator needs to be evaluated. Especially, because future designs mostly omit the coupling altogether in order to achieve a more compact design. Consequently, the torque propagation throughout the drivetrain needs to be evaluated, due to the change in torsional drivetrain behavior as a result of the missing spring damper element.

The torque excitation results during electrical faults will be validated via extensive tests with the same set up as in the simulation at the system test bench of CWD.

References

1. Rohrig K (2019) Powering the 21st century by wind energy. Appl Phys Rev. https://doi.org/10.1063/1.5089877
2. Dhanola A (2020) Tribological challenges and advancements in wind turbine bearings: a review. Eng Fail Anal. https://doi.org/10.1016/j.engfailanal.2020.104885
3. Erlich I (2007) Dynamic behavior of DFIG-based wind turbines during grid faults proc. Power Conversion Conference, Nagoya, pp 1195–1200
4. Ahmed S (2020) Grid integration challenges of wind energy: a review. IEEE Access 8:10857–10878. https://doi.org/10.1109/ACCESS.2020.2964896
5. Röder J (2021) Investigation of dynamic loads in wind turbine drive trains Due to grid and power converter faults. Energies 14:8542. https://doi.org/10.3390/en14248542
6. Bartschat A (2018) Zuverlässige Leistungselektronik für Windenergieanlagen. IWES final report. Fraunhofer Verlag
7. Duda T (2018) Investigation of dynamic drivetrain behaviour of a wind turbine during a power converter fault. J Phys 1037(5):1456–1463
8. Sheng S (2016) Wind turbine gearbox reliability database, condition monitoring, and operation and maintenance research update, Colorado
9. Röder J (2020) Simulative investigation of the load propagation in a wind turbine drive train during a power converter fault. J Phys Conf Ser 1618:32028
10. Röder J (2022) Reduction of gearbox loads of a DFIG wind turbine during grid faults with optimized converter configurations. J Phys Conf Ser 2265:32034. https://doi.org/10.1088/1742-6596/2265/3/032034
11. Herzog F (2022) Influences on the LVRT behavior of DFIG wind turbine systems. J Phys Conf Ser 2265:22075. https://doi.org/10.1088/1742-6596/2265/2/022075
12. Matzke D (2017) Full scale system simulation of a 2.7 MW wind turbine on a system test bench. In: Proc. of conf. for wind power drives Aachen, pp 241–254
13. Matzke D (2019) Validation of MBS modelling methods to calculate bearing and tooth loads in the planetary gear stage of a wind turbine. In: Proc. of conf. for wind power drives Aachen

14. Kiekbusch T (2017) Zylinderrollenlagermodul für Simpack, FVA Forschungsvorhaben Nr. 625 II. Final Report 1234. Forschungsvereinigung Antriebstechnik e.V., Frankfurt

15. Röder J (2021) Simulative investigation of wind turbine gearbox loads during power converter fault. Forsch Ingenieurwes 85:251–256. https://doi.org/10.1007/s10010-021-00461-2

16. DIN ISO 6336-20: Calculation of load capacity of spur and helical gears—Part 20: Calculation of scuffing load capacity—Flash temperature method, (2019).

17. Blok H (1937) Measurement of temperature flashes on gear teeth under extreme pressure conditions. In: Proc. Gen. Disc. Lubrication London. vol 2, pp 14–20

18. DIN ISO 6336-22: Calculation of load capacity of spur and helical gears—Part 22: Calculation of micropitting load capacity, (2018).

19. DIN ISO 6336-4: Calculation of load capacity of spur and helical gears—Part 4: Calculation of tooth flank fracture load capacity, (2019).

20. Evans R (2013) Prevention of smearing damage in cylindrical roller bearings. Tribol Trans. https://doi.org/10.1080/10402004.2013.788236

21. Van Lier H (2015) Schädlicher Wälzlagerschlupf. FVA Abschlussbericht 1124, Forschungsvorhaben Nr.663. Forschungsvereinigung Antriebstechnik e.V., Frankfurt

22. DIN ISO 21771: Gears—Cylindrical involute gears and gear pairs—Concepts and geometry, (2014).

23. Poplawski J (2000) Effect of roller profile on cylindrical roller bearing life prediction, NASA tech. Memo. Society of Tribologists and Lubrication Engineers, Tennessee

24. ISO/TS 16281:2008-06: Rolling bearings—Methods for calculating the modified reference rating life for universally loaded bearings, (2008).